FINAL REPORT

Project Title:	Deformation Microstructures and Creep Mechanisms in Advanced Zr-based Cladding under Biaxial Loading
Covering Period:	Oct 14, 2006 through July 14, 2008
Date of Report:	Aug 11, 2008
Recipient:	North Carolina State University, Raleigh NC 27695-7909
Award Number:	DE-FG07-041D14611
Subcontractors:	--------
Other Partners:	--------
Contact(s):	K. Linga (KL) MURTY, 919-515-3657, murty@ncsu.edu
Project Team:	Nancy Elizondo, US DOE, Idaho Operations Office
Project Objective:	Investigate creep behavior of Zr-based cladding tubes with attention to basic creep mechanisms and transitions in them at low stresses and/or temperatures and study the dislocation microstructures of deformed samples for correlation with the underlying micromechanisms of creep.

Report:

The research project was funded under NEER program to support nuclear engineering education and research. The project started on 7/15/2004. The grant supported a number of graduate students who took part on ¼ and ½ time bases. Along with the graduate students, a post-doctoral fellow worked on the project to assist the graduate students.

Major aim of the proposed work was to examine the transitional creep mechanisms in Zr-based alloys under biaxial loading and to characterize deformation microstructures in the various regimes. A biaxial creep tester was available in the Nuclear Materials Laboratory at NC State to perform internal pressurization of closed-end tubing samples superimposed with axial load. A Laser telemetric extensometer and an LVDT made it possible to monitor both the hoop and axial strains in-situ during creep. Along with biaxial creep tests, burst tests were performed on closed-end tubing samples at different temperatures and internal pressures yielding rupture life of Zircaloy cladding. During the tenure of the project, a second creep machine was built from the components available in the Nuclear Materials Laboratory at NC State and made operational so that creep tests under varied loading conditions can be performed. For both creep test systems, on-line strain (hoop and axial using Laser telemetric extensometer and LVDT respectively) monitoring is accomplished through Labview program on PCs. Both the creep machines are pressurized using the same pressurizer while a D/A converter and a

data acquisition system are used for on-line data monitoring and analyses. Figure 1 shows the Burst and Biaxial Creep Facility.

Figure 1 Biaxial Creep Facility
Fig. 1 Pressurizer (right front) and biaxial creep machines

Burst properties of Zircaloy were determined by internally pressurizing Zircaloy tube samples at different temperatures and internal pressures and by noting the rupture times. These studies were made as a part of MS thesis of Mr. Brian Marple entitled *"Creep Rupture Study of Annealed Zircaloy-4: Stress and Temperature Effects."* Mr. J. Yan who was working for his doctoral degree was partially supported by this grant that lead to his thesis entitled, "*Crystallographic Texture and Creep Anisotropy in Cold-Worked and Recrystallized Zirlo*." The graduate students supported by the grant also include Mr. Brad Mayhew and Mr. Srikant Gollapudi; these students received partial support from this grant while being part-time teaching assistants in the department. Dr. I. Charit, a post doctoral fellow supported by a different grant in the Nuclear Materials Group assisted the graduate students in their research.

Multiple creep-rupture tests were performed at three stations. Two of these stations were located on an ATS® Series 1815 gas pressurization system (Fig. 2a). Prior to testing, this system was extensively automated to indefinitely maintain a high pressure testing supply which was then regulated to each specimen. This was an essential feature in the performance of long-term creep-rupture testing. The furnace on this system is capable of maintaining a temperature up to 500°C. The annealing furnace also interchanges as a high temperature burst testing machine as well. Through a simple conversion process, low grade argon is used to pressurize the specimen. In series with the specimen is a pressure switch which controls a timer that records time to rupture. The two biaxial creep machines were also used to perform closed-end internal pressurization creep studies (Fig. 2b). These machines provide in-situ measurement of axial and circumferential strains at temperatures up to 900°C; Fig. 3a is a photograph of the strain measuring system. The frames are capable of imposing a 12,000 lb. axial load. A biaxial stress state (σ_θ:σ_z=2:1) is imposed by internally pressurizing the specimen. The gas pressurization system has been modified to supply both biaxial creep testing stations as well as the two burst testing stations.

The burst properties of recrystallized Zircaloy-4 tubing (Zry-4) are summarized below. Fig. 3b depicts the recrystallized grain structure. The data gathered covered stresses ranging from 27 MPa – 350 MPa and temperatures ranging from 250°C - 600°C. After each test, the specimen was removed from the test station and measurements were taken and averaged to determine the strain to rupture. The strain rate was calculated as the ratio of the uniform strain and rupture time:

$$\dot{\varepsilon} = \frac{\varepsilon_u}{t_r}$$

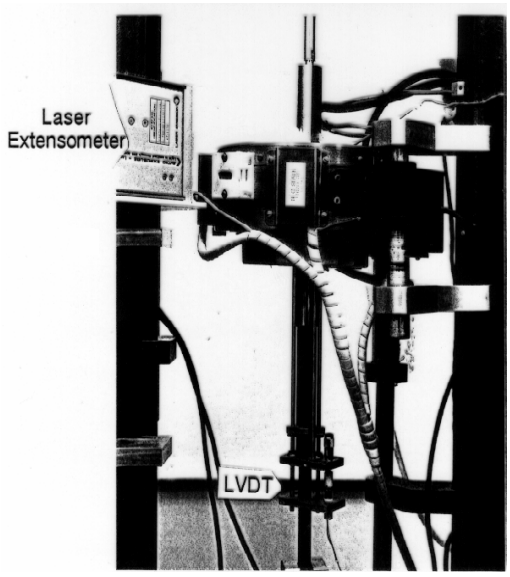

Fig. 3a. Extensometry for in-situ monitoring of diametral and axial strains

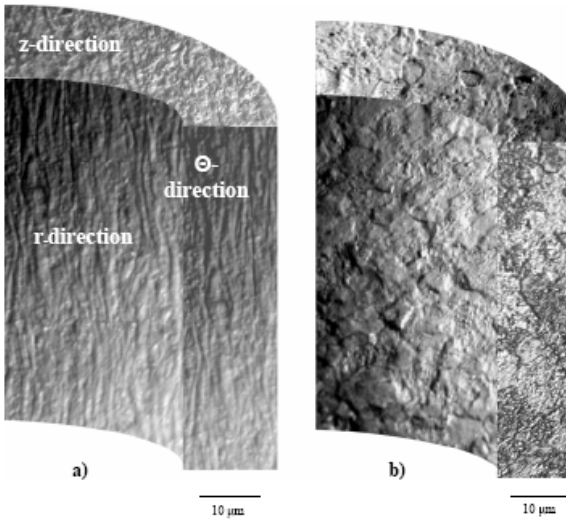

Fig. 3b. Grain structures in as-received and Rx Zry-4

Fig. 2a. Gas Pressurization

Fig. 2b. Biaxial Creep Machine

Figure 4 depicts isothermal burst data shown as hoop stress versus rupture time at varied temperatures. Larson-Miller parameter (LMP) was calculated from these data,

$$LMP = T\,(\log t_r + 20)$$

with T in K and t_r in hours. Figure 5 is the corresponding LMP plot and we note an excellent correlation. Earlier data from Zhou and Mayuzumi are included for comparison.

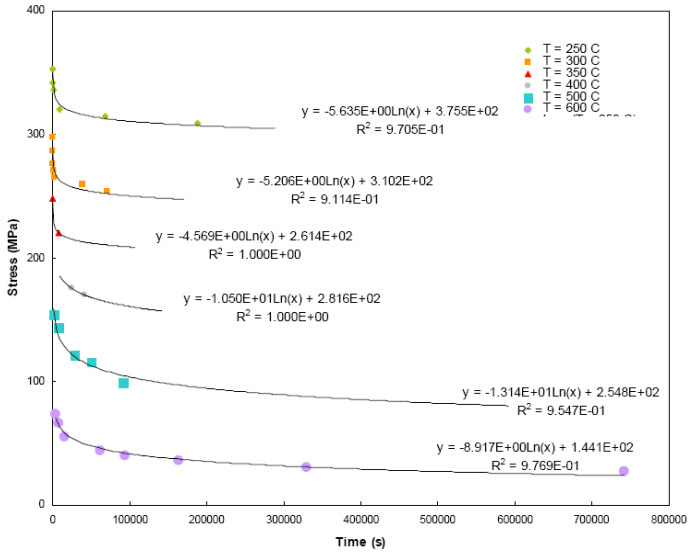

Fig. 4. Hoop Stress vs Rupture Time for Rx Zry-4

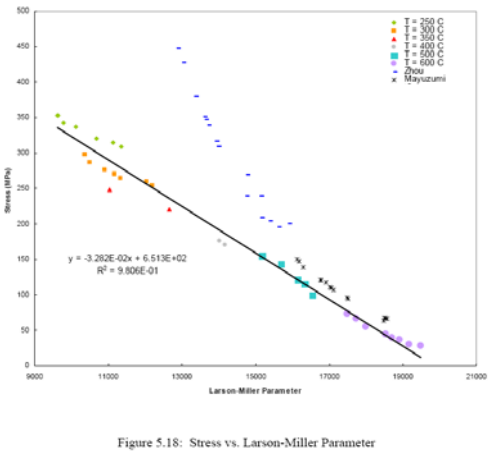

Figure 5.18: Stress vs. Larson-Miller Parameter

Fig. 5. Stress vs LMP for Rx Zry-4

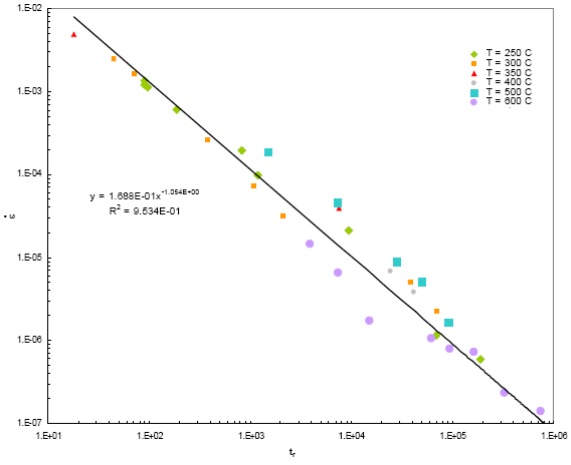

Fig. 6. Strain-rate vs rupture time for Rx Zry-4 depicting the Monkman-Grant relationship

The rupture time is seen to vary inversely with the hoop strain-rate evaluated using the above equation as shown in Figure 6:

$$\dot{\varepsilon} t_r = \kappa\,.$$

where κ is the material constant. These data in addition enabled an evaluation of other relevant parameters describing strain-rate as a function of test temperature and applied

stress. The strain-rates are plotted versus the applied stress in Figure 7 as a semi-log graph indicating the exponential stress dependence of the strain-rate:

$$\dot{\varepsilon} = A' e^{B\sigma/E} = Ae^{-Q/RT} e^{B\sigma/E} .$$

Here, Q is the activation energy for deformation, E the temperature dependent elastic modulus, A and B are constants. The activation energy was determined from the Arrhenius plot of A' versus 1/T as shown in Fig. 8 that gave an activation energy value of 58.934 kCal/mole which is in close agreement with that for self diffusion.

One can then relate the normalized strain-rate to the normalized stress as shown in Figure 9 and we note that the data exhibit a sharp change in the slope indicating a possible change in the underlying deformation mechanism. This is significant in the sense that the standard Monkman-Grant relation as depicted in 6 does not show such transition. This transition is due to the breakdown of the power-law at high stresses and is clearly shown in Fig. 10 where the normalized strain-rates are plotted versus normalized stress in a double-log format that clearly exhibits the transition from power-law to exponential stress dependence.

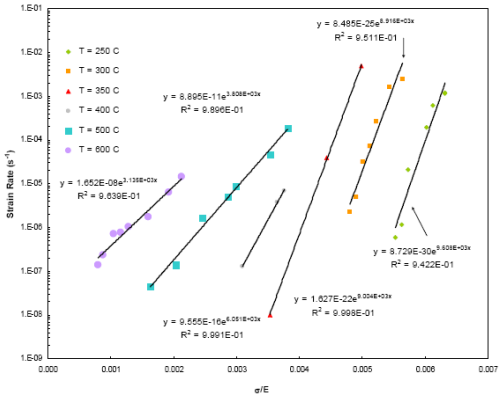

Fig. 7. Semi-log plot of strain-rate vs stress

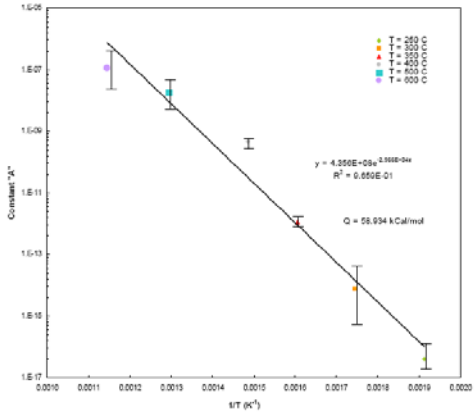

Fig. 8. Arrhenius plot for activation energy

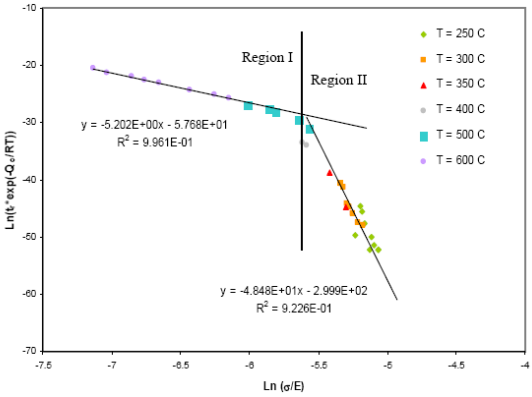

Fig. 9. Normalized strain-rate vs rupture time

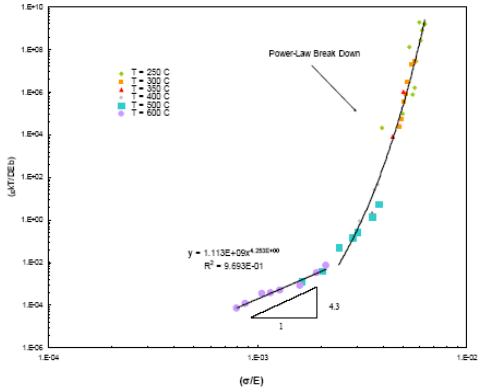

Fig. 10. Double-log plot of normalized strai-rate vs stress

Thus in region I at low stresses the power-law holds:

$$\dot{\varepsilon} = A'\left(\frac{\sigma}{E}\right)^n = Ae^{-Q/RT}\left(\frac{\sigma}{E}\right)^n \quad \text{region I (low-stresses).}$$

In terms of normalized strain-rates using Dorn parameters we find,

$$\frac{\dot{\varepsilon}kT}{DEb} = A\left(\frac{\sigma}{E}\right)^n \text{ - region I.}$$

Figure 10 is a double-log plot of normalized strain-rate versus normalized stress that revealed power-law at low stresses with a stress exponent of 4.25 while at higher stresses an exponential stress dependence is noted. These data clearly point to the fact that deformation in Zry-4 is due to the climb of edge dislocations as per the class-M behavior with the distinct power-law breakdown at higher stresses ($>10^{-3}$E).

While MS thesis of Mr. Marple contains detailed information on optical microscopy, crystallographic textures and microstructures using electron microscopy, we will summarize notable information on TEM microstructures following burst. Dislocation microstructures observed in Region I and Region II are emphasized. Region I corresponding to the power-law breakdown exhibited subgrain formation as depicted in Figures 11.

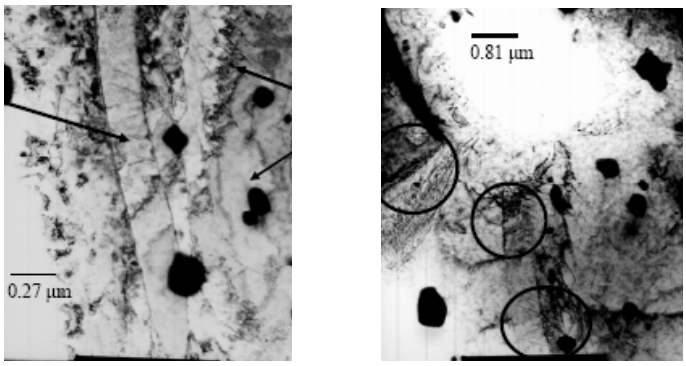

Fig. 11a. Dislocation microstructures in region I (600C, 27.5MPa)

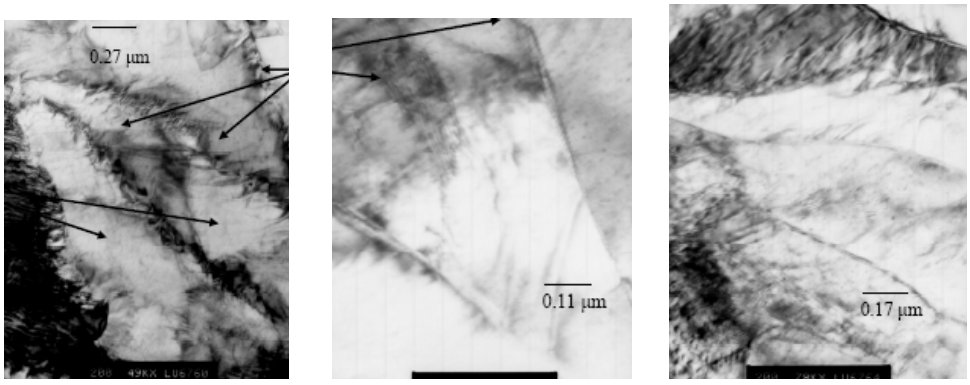

Fig. 11b. Dislocation microstructures in region I (500C, 115.8MPa)

In the high stress regime corresponding to power-law breakdown region (II), randomly distributed dislocations are noted (Figures 12). These observations are seen to be essentially similar to those reported in a Ti alloy (G. Srikant, B. Marple, I. Charit and K.L. Murty, "Characterization of stress rupture behavior of cp-Ti via burst testing," Mat Sci Eng.

A463, 2007, pp. 203-207). The results reported here were presented at 2005 ANS Winter meeting in Washington, DC; the summary is given below:

"Short-Term Rupture and Biaxial Creep Studies of Recrystallized Zircaloy-4 Tubing"

B. Marple, I. Charit, K.L. Murty
North Carolina State University, Raleigh, NC 27695 USA

Summary

In most PWR applications, Zircaloy-4 has been replaced by new alloys such as M5™ & Zirlo™, which have been developed by Framatome-ANP and Westinghouse, respectively. However, Zicaloy-4 is still valuable for use in low burn-up cores. Most importantly, for the open fuel cycle currently used in the U.S., Zircaloy-4 will be the primary barrier for spent PWR fuel in the Yucca Mountain repository. Hence, it is very important that we understand the fundamental mechanisms of creep in the fuel cladding at low stresses. It has been shown that blind extrapolation using short-term creep data would be non-conservative over an extended period because other creep mechanisms may become relevant at low stresses. This work could also be adapted to the new alloys currently in use because the change in the mechanism from in-pile creep to the mechanism(s) dominant over years of dry-storage will, most likely be the same, although it will occur at different temperatures and stress levels.

The tubing was recrystallized at 700°C for 4 hours in order to avoid the recovery processes that would occur in cold-worked tubing at creep tests above 400°C (the minimum temperature at which cold-worked Zr-4 is typically stress relieved). Biaxial creep testing has been underway on recrystallized Zircaloy-4 tubing at temperatures ranging from 500°C to 600°C and at varied stresses ranging from $2x10^{-4}E$ to $5x10^{-3}E$. Although such high temperatures are never seen in normal service and especially in dry-storage, they were necessary to shorten the length of the creep tests to a reasonable time. Both the axial and diametric strains are measured in situ and the steady state creep rate is determined. The activation energy and stress exponent will be determined from the steady-state creep-rate data which will help to identify the underlying deformation mechanism.

Rupture tests using internal pressurization are also performed on the recrystallized Zircaloy-4 tubing at temperatures ranging from 250°C to 600°C. After rupture, the uniform circumferential elongation is measured so that the strain rate can be estimated. These results will be compared with biaxial creep data. The burst test data will be analyzed in terms of Larson-Miller parameter as well as the Monkman-Grant relation that will be helpful in making long-term predictions at service and dry-storage conditions. Transmission electron microscopy (TEM) will be used to characterize the dislocation microstructures that will aid in identifying the creep mechanism.

Plans include texture studies on the recrystallized material so that the effects of preferred grain orientation can be correlated to the creep anisotropy. The texture analysis will be used to evaluate the anisotropy parameters, R & P, which should correlate to the differential strain rates in the hoop and axial directions obtained from creep tests for a given loading condition. The crystalline orientation distribution function or CODF will be determined from the texture data so that the anisotropic creep behavior of the textured bulk polycrystalline material can be predicted.

The work is supported by DOE-NEER program through grant # DE-FG07-041D14611. Acknowledgements are due to Dr. J. Yan and Mr. S. Gollapudi for assistance and comments.

Anisotropic biaxial creep studies on Zry-4 and Zirlo were taken up by Mr. J. Yan supported partly by this grant. The results were presented at the Materials Science & Technology conference in Pittsburgh (MS&T 2005) and published in the proceedings. The paper is reproduced below.

Effects of Alloying and Thermal Treatment on Creep Anisotropy of Zircaloys: Application to In-Reactor Performance

Indrajit Charit, Jinyuan Yan, Brian Marple and K. Linga Murty
North Carolina State University
Raleigh, NC 27695-7909, USA

Keywords: Zircaloys, Niobium Addition, Texture, Creep Anisotropy, Cladding Life

Abstract

Zr-based alloys are commonly used as thin-walled tubing to clad nuclear fuel, and their reliability during in-reactor operation is of paramount importance. Also of great concern, is the long-term performance of the fuel cladding after irradiation because it will be the primary barrier of the spent fuel during long-term dry storage. While standard Zircaloys have been in use for quite some time, recent emphasis on high burn-up applications led to additions of Nb to improve corrosion and oxidation resistance. These cladding tubes are used in both cold-worked stress-relieved (CWSR) and completely recrystallized conditions. We summarize here the effect of recrystallization on crystallographic texture and creep anisotropy of Zircaloy-4 (Zr alloyed with Sn and Fe) and Nb-added Zircaloy. Crystallographic textures are characterized using direct pole figures from which the crystallite orientation distribution functions (CODF) are evaluated. Predictions based on CODF combined with slip models are compared with the experimental results on strain-rate ratios and creep loci at constant energy dissipation. Deviations from prism slip models in CWSR are believed to arise from grain shape anisotropy, and stress enhancements during GBS are considered to quantify these effects. The utility of mechanical anisotropy parameters is described to predict the dimensional changes in-reactor. A limited amount of results obtained to-date on the transitions in creep mechanisms with applied stress and temperature reveal possible dangers in *blind* extrapolation of the short-term high-stress data to long-term low stress conditions.

Introduction

Zirconium alloys have traditionally been used as structural materials for various applications in the fuel assemblies of fission reactors. These include thin-walled tubes to clad radioactive fuel pellets, spacer grids and mixing channels for light water reactors (LWR), and pressure and calandria tubes for heavy water reactors (HWR). Zircaloys are Zr-based alloys with tin (Sn) and iron (Fe) as the main alloying elements. However, minor amounts of Ni, Cr, and O are usually present. Readers interested in the history of Zircaloy development are referred to Ref. [1].

Zircaloys used as a thin-walled cladding material are subjected to complex multi-axial stress states at elevated temperatures because of internal pressurization from fission products, external pressure and flow of the coolant, and various other factors, including the interaction of the expanding fuel pellets with the tubing [2]. Zircaloys have a hexagonal close-packed (hcp) crystal structure with low c/a ratio and limited number of slip systems. During fabrication of these tubes, they tend to form strong texture. Consequently, the creep behavior of the Zircaloy tube becomes complex and anisotropic in nature. Thus, the precise prediction of dimensional changes under in-reactor conditions becomes difficult. Further, many critical texture-dependent phenomena like stress corrosion cracking (SCC), hydride formation, radiation growth etc. take place simultaneously [3].

The identification of deformation mechanism is an important aspect in creep life prediction. Zircaloys generally show M-type creep behavior with stress exponent (n) values of 5-7 [4]. However, as the stress level is changed, transitions in creep behavior are noted. Newtonian viscous or diffusional creep (stress exponent, n=1) occurs at lower stress levels. Thus, the creep anisotropy is also influenced by the underlying micromechanisms involved. Furthermore, the microstructural conditions (whether cold worked or recrystallized) also influence the creep anisotropy.

The recent trend in the development of Nb-modified zirconium alloys (Zirlo[TM(i)], M5[TM(ii)]) with superior corrosion and oxidation resistance has necessitated a detailed evaluation of their creep properties. An investigation with Zirlo (which has a composition close to Zircaloy-4 with addition of ~1.0 wt.% Nb) has shown that it behaves like an A-type alloy, i.e., it shows a viscous glide creep regime with n=3 at intermediate stress levels [5]. However, with some recent developments in cladding technology like the use of composite barrier cladding, it becomes more complicated to predict cladding life in-reactor.

(i) Zirlo is a trademark of Westinghouse Electric Company
(ii) M5 is a trademark of Framatome ANP

In this study, we demonstrate the effect of alloying and thermal treatment on the texture and creep anisotropy for this important class of materials. Two alloys, Zircaloy-4 and Zirlo, in two different microstructural conditions (cold worked stress relieved, CWSR and recrystallized, RX) were considered in this study. Different formalisms of creep anisotropy relevant to zirconium alloys and transitional deformation mechanisms are described using results from both materials.

Materials and Microstructural Characteristics

Table I gives nominal compositions of as-received thin-walled cladding tubes of Zircaloy-4 and Zirlo, which were received in CWSR condition. Figures 1a and b show the microstructures of CWSR and Rx Zircaloy-4 alloy tubings in three orthogonal sections. The CWSR microstructure is elongated along the axial direction bearing the evidence of the fabrication process (tube extrusion). However, after recrystallization anneal (873 K / 4 hours), equiaxed grains with an average diameter of ~18 μm were formed. A similar microstructural evolution was observed in Zirlo following recrystallization (873 K / 4 hours), as revealed in Figures 2a and b. The average grain size for recrystallized Zirlo is ~20 μm.

Table I. Chemical Compositions of Zr alloys Investigated (in wt.%)

Element	Sn	Fe	Cr	Nb	O	Ni	Zr
Zircaloy-4	1.2-1.7	0.18-0.24	0.07-0.13	-	0.09-0.13	<0.007	Balance
Zirlo	0.9-1.2	0.1	<0.01	0.9-1.13	0.090-0.15	<0.007	Balance

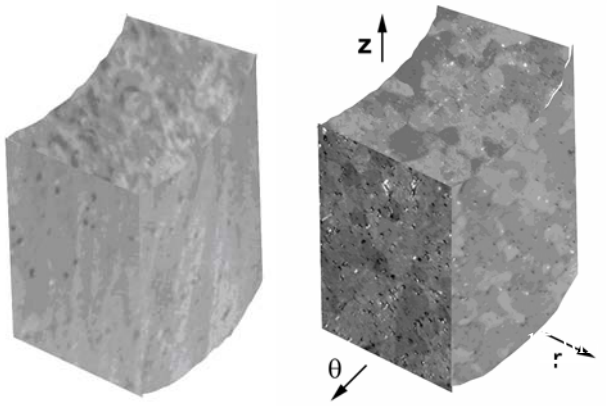

(a) (b)

Figure 1. Microstructure of Zircaloy-4, (a) CWSR, (b) RX.

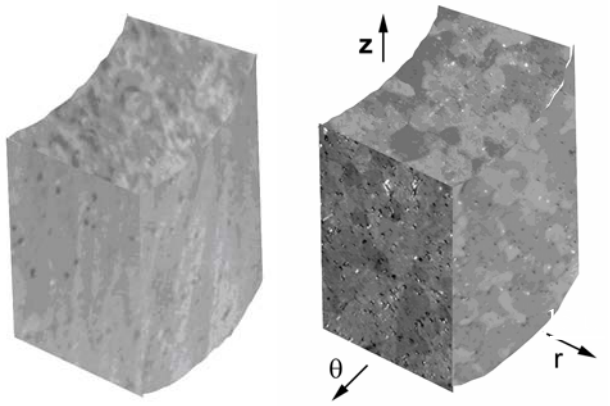

(a) (b)

Figure 2. Microstructure of Zirlo, (a) CWSR, (b) RX.

Crystallographic Texture

Commonly, crystallographic texture is represented by inverse and direct pole figures. In this study, x-ray diffraction was used on x-ray 'composite' specimens (slices stacked together) along three orthogonal directions, z (axial), radial (r) and hoop (θ) for obtaining pole figure data. The inverse pole figure is a stereographic projection depicting the relative intensities of different diffracting planes for a particular sample direction. On the other hand, the direct pole figure is a stereographic projection, which shows the variation of pole density with pole orientation for a particular set of crystallographic planes. These figures are drawn by plotting iso-intensity contours in the unit of 'times random' intensity. Direct pole figure data are needed in the determination of CODF and slip-dominated predictions. In this paper, we present basal and prism pole figures for Zircaloy-4 and Zirlo (Figure 3). Close examination of the pole figures for Zircaloy-4 reveals that the basal pole figure shows typical bimodal distribution of basal poles with peaks at around $\pm 35^{o}$ from the radial toward the hoop direction. For the CWSR Zircaloy-4, the prism poles are clustered around the axial direction. However, in the recrystallized Zircaloy-4, the prism poles rotated by $\pm 30^{o}$ from the axial direction toward the hoop direction. This rotation is thought to have a significant effect on creep anisotropy. For Zirlo, a similar trend has been noticed in CWSR and recrystallized materials [6]. So, it can be stated that the recrystallization anneal treatment has minimal effect on basal pole distribution, whereas the prism pole distribution is significantly affected.

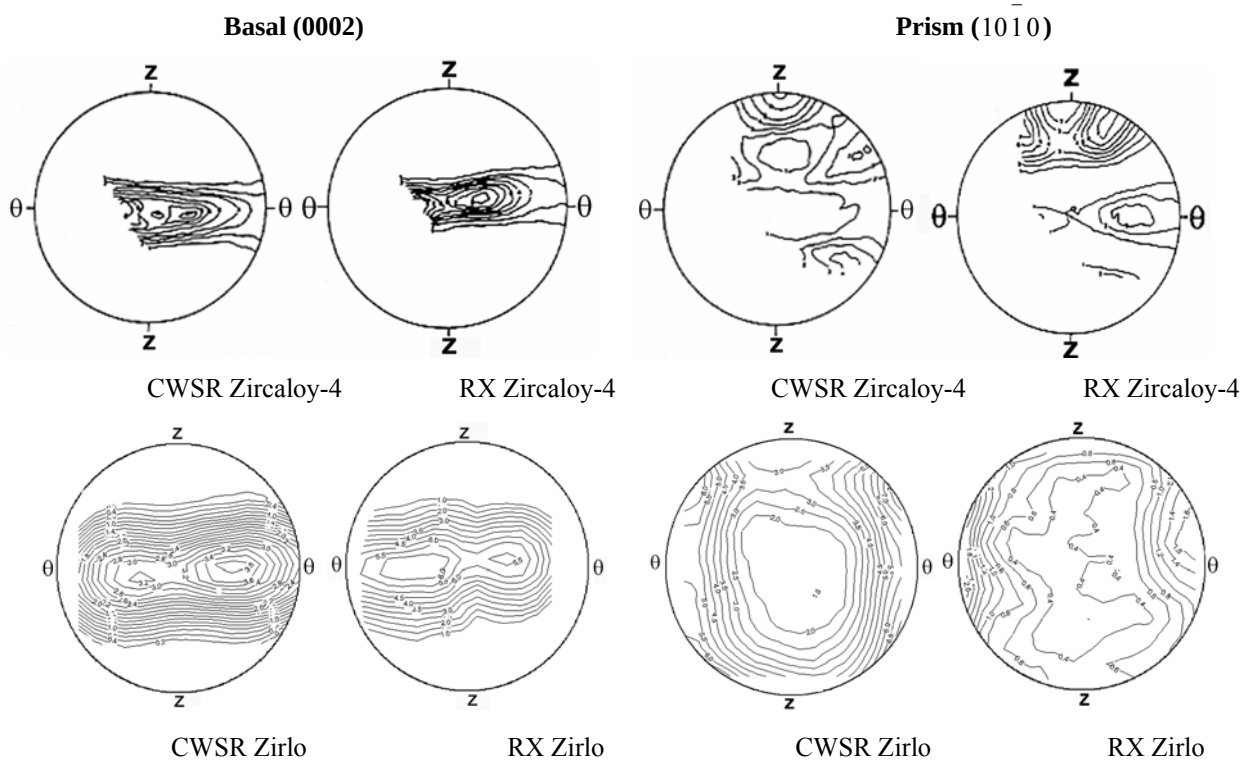

Figure 3: Basal and prismatic direct pole figures for Zirlo and Zircaloy-4 under CWSR and RX conditions.

Quantitative characterization of texture can be accomplished through the determination of a distribution function representing the probability that a crystallite will lie in a certain range of orientations with respect to some fixed reference coordinates. The probability that a crystallite has an orientation (θ,ψ,ϕ) with respect to the specimen axes is expressed as a series of generalized spherical harmonics [7],

$$\omega(\theta,\psi,\phi) = \sum_{l=0}^{\infty} \sum_{m=-l}^{l} \sum_{n=-l}^{l} W_{lmn} Z_{lmn}(\cos\theta) e^{-im\psi} e^{-in\phi} , \quad (1)$$

where W_{lmn} are the appropriate series coefficients and Z_{lmn} are the augmented Jacobi polynomials. This probability function $\omega(\theta,\psi,\phi)$ is known as the Crystallite Orientation Distribution Function (CODF) and (θ,ψ,ϕ) are Euler angles connecting coordinate axes embedded in the crystallite with axes coincident with the specimen and the principal working directions of the material. More details about the CODF evaluation can be found elsewhere [8]. The orientation distribution functions are calculated corresponding to the pole figures, which are illustrated in the form of Euler plots at constant intervals (5^o) of ϕ, which is the angle of rotation around c-axis of the hcp crystal. Figure 4 shows the Euler plots for CWSR and RX Zircaloy-4 materials. The Euler plots for CWSR and RX Zirlo materials have quite similar features [6]. These Euler plots represent the fraction of crystals oriented in a particular direction specified by the Euler angles, and $\theta = 0^o$ and $\psi = 0^o$ referring to the axial direction, $\theta = 90^o$ and $\psi = 90^o$ refer to the hoop, while $\theta = 90^o$ and $\psi = 0^o$ refer to the radial directions of the tubing. However, the utility of these plots is in the characterization of the ϕ-dependence of the ideal orientations, (hk.l) & <uv.w>, where (hk.l) refers to the crystallographic planes lying in the plane normal to the radial direction (i.e. z-θ plane) and [uv.w] is a crystallographic direction in this plane along the axial direction. The ideal orientations corresponding to the peak positions can thus be calculated in different ϕ sections. The Euler plots are shown up to the ϕ value of 55^o as the hexagonal symmetry introduces repetition after that.

Use of crystallographic texture in terms of CODF brings with it the advantage of predicting mechanical properties of bulk polycrystalline materials quantitatively based on suitable information from single crystals. To a reasonable degree, the bulk

property is related to the microscopic property by statistical averaging using the CODF so that the average property of the polycrystalline aggregate, $<\rho(\theta,\psi,\phi)>$, is given by [7-9]

$$<\rho(\theta,\psi,\phi)> = \int_0^{2\pi}\int_0^{2\pi}\int_{-1}^{1} \rho(\theta,\psi,\phi)\ \omega(\theta,\psi,\phi)\ d(\cos\theta)\, d\psi\, d\phi \tag{2}$$

As will be clear afterwards, CODF is used to predict the strain rate ratios, in other words, to evaluate creep anisotropy. Thus, the property of interest is the strain rate of the textured, bulk material evaluated from the information on single crystal due to the relevant slip system(s) active in a particular crystal structure.

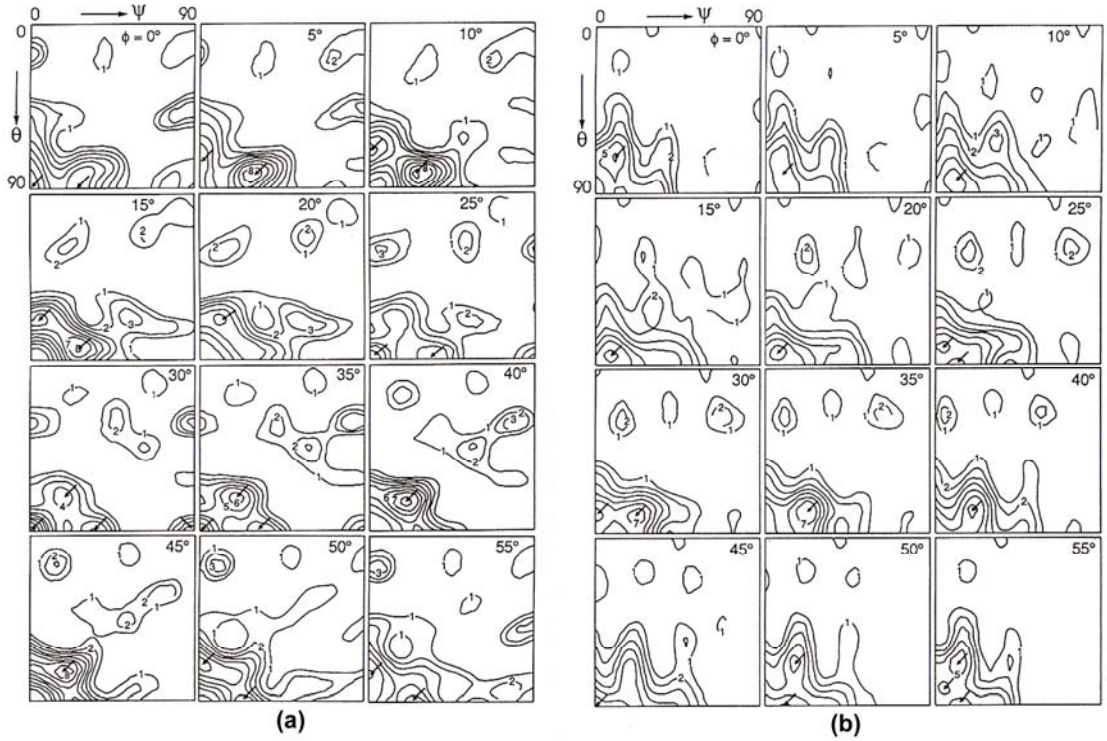

Fig. 4: Euler plots at constant ϕ, the rotation around c-axis from 0^o to 55^o at 5^o intervals; for (a) CWSR Zirlo and (b) RX Zircaloy-4.

Creep Anisotropy – Fundamental Relationships

Following Hill's equation [10] and later modifications by Backofen et al. [11], anisotropic biaxial creep can be characterized by defining a generalized stress (σ_g), given by

$$\sigma_g^2 = \frac{R(\sigma_r-\sigma_\theta)^2 + RP(\sigma_\theta-\sigma_z)^2 + P(\sigma_z-\sigma_r)^2}{P(R+1)} \tag{3}$$

where σ_θ is the hoop stress, σ_z the axial stress, σ_r the radial stress, and R and P are the anisotropy parameters, which depend on crystallographic texture. For thin-walled tubing with $\sigma_r = 0$, the above relation gets simplified into

$$\sigma_g = \left(\frac{R\alpha^2 + (\alpha-1)^2 RP + P}{P(R+1)}\right)^{\frac{1}{2}} \sigma_z \tag{4}$$

where α (σ_θ/σ_z) is the stress ratio.

Using Prandtl-Reuss energy balance equation in conjunction with the above yield criterion, the strain rates (or strain) in three orthogonal directions can be expressed as

$$\begin{bmatrix} \dot{\varepsilon}_r \\ \dot{\varepsilon}_\theta \\ \dot{\varepsilon}_z \end{bmatrix} = \frac{\dot{\varepsilon}_g}{P(R+1)\sigma_g} \begin{bmatrix} (R+P) & -R & -P \\ -R & R(P+1) & -RP \\ -P & -RP & P(R+1) \end{bmatrix} \begin{bmatrix} \sigma_r \\ \sigma_\theta \\ \sigma_z \end{bmatrix} \tag{5}$$

where $\dot{\varepsilon}_g$ is the generalized strain rate corresponding to σ_g above. It is evident from the above equations that R and P are the anisotropy parameters. These anisotropy parameters are influenced by textural characteristics. Using the Prandtl-Reuss energy balance equation with the yield criterion (Eqn. 3), the anisotropy parameters can be expressed as transverse contractile strain (rate) ratios [12]:

$$R = \left(\frac{\varepsilon_\theta}{\varepsilon_r}\right)_{\varepsilon_z} \text{ when } \sigma_\theta = \sigma_r = 0, \text{ and } P = \left(\frac{\varepsilon_z}{\varepsilon_r}\right)_{\varepsilon_\theta} \text{ when } \sigma_z = \sigma_r = 0. \tag{6}$$

For the special case of thin-walled tubing, the ratio of strain rates along the hoop and axial directions is given by

$$\beta = \frac{\dot{\varepsilon}_\theta}{\dot{\varepsilon}_z} = \frac{(P+1/P)\alpha - 1}{(R+1)/R - \alpha} \tag{7}$$

Thus, three useful relations essential for the evaluation of R and P can be expressed by

$$\beta = \frac{R}{P}, \text{ for equi-biaxial loading (i.e. } \alpha=1), \tag{8a}$$

$$\rho = \frac{\dot{\varepsilon}_\theta}{\dot{\varepsilon}_r} = \frac{-\beta}{\beta+1} = R, \text{ for uniaxial loading } (\alpha=0) \tag{8b}$$

$$P = \frac{\alpha}{1-\alpha} \text{ for } \rho = 0. \tag{8c}$$

Biaxial Creep Testing - Methodologies and Results

The creep anisotropy of zirconium alloys is best investigated using biaxial creep tests of thin-walled tubes. In that, an axial load is superimposed with internal pressurization. Further, the anisotropy in Zircaloys is clearly revealed by creep testing under equi-biaxial stress state (i.e. the ratio of hoop stress to axial stress being 1). The specimen temperature was maintained within ±1 K. The axial displacement was measured in situ using an LVDT extensometer, while the change in tube diameter was monitored using a laser micrometer. An appropriate algorithm was developed to continuously monitor the axial and hoop strains during creep testing. The stresses to be applied were calculated using appropriate equations [8]. Typical creep curves (axial and hoop strains vs. time) for Zircaloy-4 under equi-biaxial (i.e. stress ratio α = 1) conditions are shown in Figure 5. Extensive creep anisotropy was noted in the hoop direction, which was significantly weaker. On the other hand, it is interesting to note that the hoop direction becomes slightly stronger in RX Zircaloy-4. Similar trends have also been noted in Zirlo [6].

Figure 6a shows the variation of the strain rate ratio (ρ) as a function of stress ratio (α) in CWSR Zircaloy-4. Using the relations in Eqn. 8, R and P parameters are measured to be 1.42±0.15 and 0.43±0.08, respectively. These data compare well with the previous results obtained by other researchers [13]. In RX Zircaloy-4, they are found to be 1.7 and 4.66, respectively [8]. Also, the ratio of hoop strain rate to axial strain rate is calculated to be

$$\beta = \left(\frac{\dot{\varepsilon}_\theta}{\dot{\varepsilon}_z} \right)_{1:1} = 3.3 \text{ for CWSR and } 0.45 \text{ for RX Zircaloy-4.} \quad (9a)$$

In CWSR Zirlo, R and P parameter values are calculated to be 0.98 and 0.43, respectively (Figure 6b), whereas after full recrystallization, the parameters change to 1.28 and 1.5, respectively. Hence, P parameter increases upon recrystallization in both the materials, but the trend in R is not so. In Zirlo, the β ratios under equi-biaxial loading are given by

$$\beta = \left(\frac{\dot{\varepsilon}_\theta}{\dot{\varepsilon}_z} \right)_{1:1} = 2.28 \text{ for CWSR and } 0.85 \text{ for RX Zirlo.} \quad (9b)$$

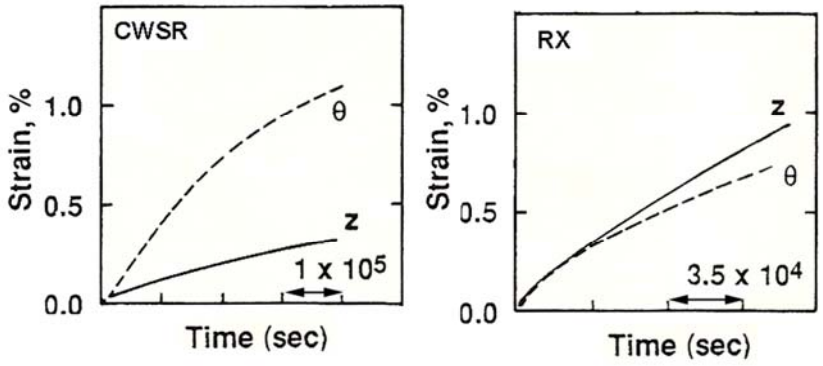

Figure 5. Creep curves for (a) CWSR and (b) RX Zircaloy-4 tubings.

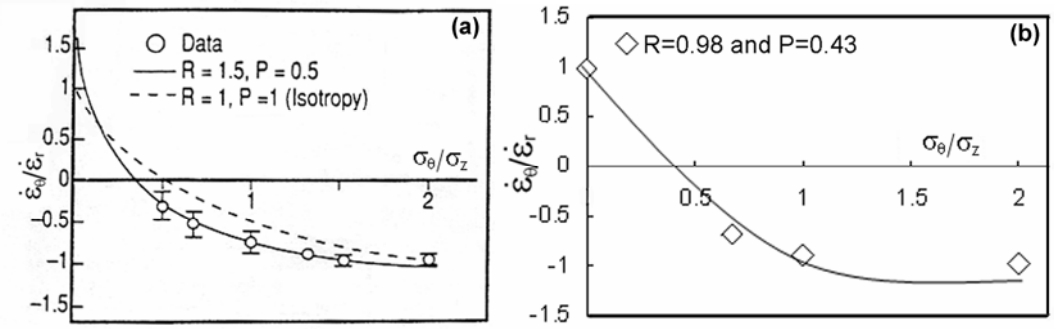

Figure 6: Strain rate ratio (hoop strain rate to axial strain rate) vs. stress ratio in CWSR (a) Zircaloy-4 and (b) Zirlo.

Therefore, the hoop direction is weaker in the CWSR condition for both Zircaloy-4 and Zirlo compared to the recrystallized ones. In fact, in the recrystallized ones hoop direction is slightly stronger than the axial direction. This observation illustrates the importance of heat treatment and the resulting texture on mechanical anisotropy. As such, it seems that the presence of Nb does not have much effect on it.

Generally, the steady state creep rate can be expressed as a function of stress via the following power law equation:

$$\dot{\varepsilon}_i = A\sigma_i^{\,n}, \text{ i} = \theta \text{ or z.} \quad (10)$$

where n is the stress exponent dependent on particular deformation mechanism operating. For RX Zircaloy-4, the variation of steady state strain rate as a function of stress under uniaxial loading is shown in Figure 7a. Transitions in deformation mechanisms can be noted. The dislocation climb-controlled flow (n = 5) occurs in the intermediate stress ranges, whereas diffusional creep regime (n =1) appears at very low stresses. At very high stresses, power law breakdown regime occurs where the creep rate changes as an exponential function of stress. Interestingly, in Zirlo a viscous dislocation-glide controlled regime (n=3) appears between the diffusional creep and dislocation climb-controlled regimes, and it has been attributed to the dislocation dragging effect caused by Nb solutes present in the alloy (Figure 7b) [5].

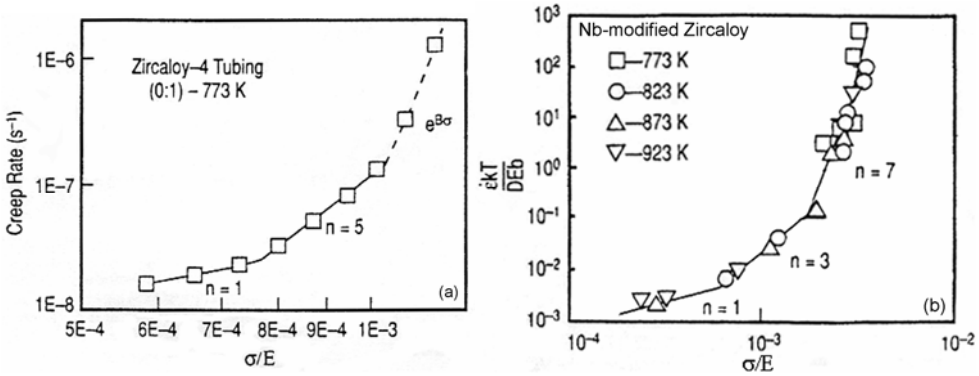

Figure 7: Evaluation of stress exponent for Zircaloy-4 and Zirlo.

A better characterization of creep anisotropy can be made through the evaluation of creep loci at constant dissipation energy rate [14]

$$\dot{W} = \sigma_\theta \dot{\varepsilon}_\theta + \sigma_z \dot{\varepsilon}_z \,. \tag{11}$$

Double logarithmic plots of the dissipation rates vs. axial stresses for different stress ratios (0-2) were made. The slope of the fitted straight lines turns out to be (n+1). At a constant dissipation energy rate, the principal stresses (σ_z and σ_θ) corresponding to the equivalent dissipation energy rate are evaluated from these plots. A creep locus is defined as the relation between the principal stresses at an equivalent dissipation energy rate. Figure 8a shows creep loci plotted at a dissipation energy rate of 8 $Jm^{-3}s^{-1}$ for CWSR and RX Zircaloy-4. The data from the study of Stehle et al. [13] on RX Zircaloy-4 are also included in Figure 8a. The effect of cold work is clearly delineated from the shape and the relative position of the creep loci. Overall, both the loci show deviation from isotropy. Similarly, in Figure 8b creep loci for Zirlo have been shown and the trend is quite similar to Zircaloy-4. The creep loci for Zirlo, however, are plotted at a dissipation rate of 5 $Jm^{-3}s^{-1}$.

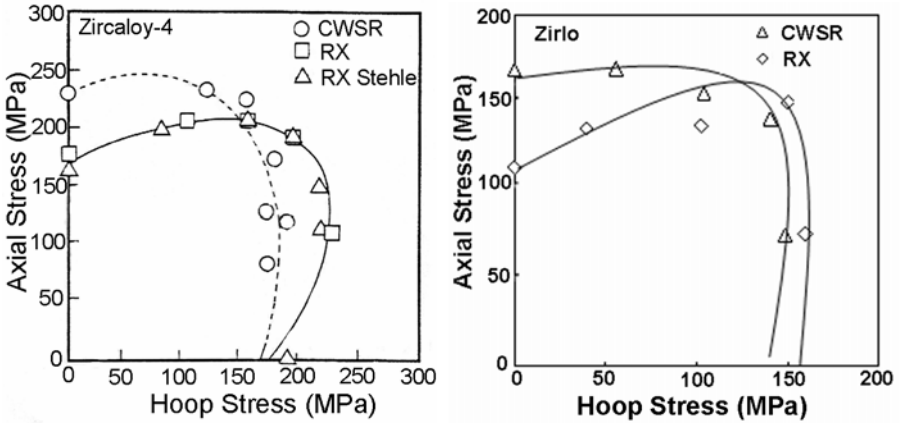

Figure 8: Creep loci for (a) Zircaloy-4 and (b) Zirlo.

CODF-Creep Model

Deformation by slip is considered along with CODF to predict creep anisotropy for the materials and textures. Once the orientation distribution of crystallites in the polycrystalline materials is evaluated and the appropriate CODF is known, the crystallite behavior in each orientation can be weighted by volume fraction of crystallites in that orientation in such a way that the polycrystalline behavior can be predicted. Using information on the probable operating slip modes in the materials, the deformation behavior of the individual crystallites as well as the polycrystalline aggregate can be predicted. Rigid body analyses like Sachs, Taylor and Bishop-Hill are utilized to predict the low temperature deformation behavior where specific slip systems are thought to operate [9]. Stress equilibrium is satisfied in lower-bound estimates. However, strain compatibility among crystallites is not considered. It has been shown that lower-bound models are also appropriate for describing high temperature creep behavior. Power-law creep is applicable to many materials including the hcp materials, and the shear strain rate in the k-th slip system is given by

$$\dot{\gamma}^k = A\left[\frac{\tau^k}{\tau_o^k}\right]^n \tag{12}$$

where A is the reference strain rate which is dependent on the test temperature, τ_o^k reference shear stress acting on the k-th slip system, and n is the stress exponent. The total strain rate is given by the total sum of the contribution from each of the active slip systems. Further details of the analysis are described elsewhere [9]. It is important to note that in the lower-bound models, the stress state in each crystallite is equated to the macroscopic stress state. The bulk creep rate is then evaluated by averaging the creep rate of the individual crystallites, weighted by CODF according to Eqn. 2.

In metals with hcp crystal structure, three different slip modes are generally considered: basal ({00.1},<11.0>), prismatic ({10.0}<11.0) and pyramidal ({11.2}<11.3>). Reference stress values are so chosen that the contribution of individual or a combination of slip systems is considered in the analysis. It is well established that the prismatic slip mode is the preferred slip mode in hcp metals with low c/a ratio (1.589 for Zr) at room temperature and above. Hence, for an instance, the reference stresses for the basal and pyramidal slip systems are taken as 1000 times as that of the prism slip system to evaluate the contribution of the prismatic slip. It is well established that the dislocation activity in these materials is limited only on prismatic slip systems [15]. It is important to note here that all slip modes contribute to the total deformation while the prism slip operates as the dominant deformation mode.

Effect of Grain Shape on Creep Anisotropy

In this section, we discuss about the role of grain shape anisotropy on the creep behavior of Zircaloys. Experimentally evaluated creep locus of RX Zircaloy-4 is compared with the creep locus predicted on the basis of prismatic slip dominance, and there exists an excellent correlation between the experimental and predicted loci, confirming the validity of the texture model used [8,16,and 17]. On the contrary, the experimental creep locus of CWSR Zircaloy-4 deviates grossly from the locus predicted by the prismatic slip model (Figure 9). Similar trend has also been noticed in Zirlo [6]. Murty et al. [16,17] showed that a good correlation for the CWSR Zircaloy can be obtained by considering stress enhancement occurring in the hoop direction during grain boundary sliding.

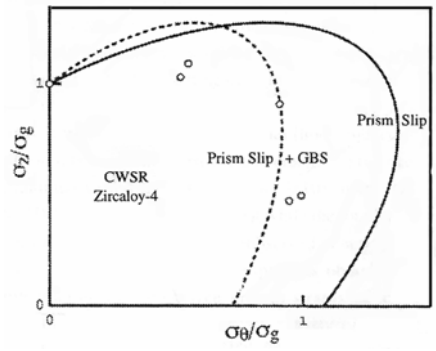

Figure 9: Experimental creep locus for CWSR Zirecaloy-4 compared with predictions based on prism slip prediction along with that predicted from imposed grain-shape effects (σ_g is the generalized stress as given by Eqn. 3).

Effects of Radiation Exposure

So far, we discussed textural characteristics and thermal creep behavior of Zircaloys. Now, it is important to consider how the creep behavior of Zircaloys is influenced by the neutron irradiation. Mechanical anisotropy of RX and CWSR Zircaloy is affected differently. As it is well known, exposure to neutron irradiation leads to a higher density of point and line defects as well as defect clusters, which are responsible for radiation hardening and embrittlement. A few studies have been devoted to understanding mechanical anisotropy of recrystallized Zircaloys after the radiation exposure, and it was noted that the pyramidal slip might become a secondary slip system along with the primary prismatic slip system [18]. Thus, the hardening of the basal plane assuming equal ease of prismatic and pyramidal slip leads to the prediction of creep loci that correlates well with the experimental data in RX Zircaloy-4 [8]. It has also been confirmed that mechanical anisotropy decreases toward isotropy in irradiated RX Zircaloys [19]. On the other hand, minor effects of neutron irradiation have been noted on creep anisotropy of CWSR cladding. Analysis by Clevinger et al. [20] revealed that the total strain tensor was different from those

observed in out-of-pile crept samples, but the creep components obtained after deducting the contribution of stress-free radiation growth strains of in-pile samples matched closely with that of the out-of-pile creep strains. Thus, it was concluded that the creep anisotropy is not significantly affected by neutron radiation exposure in CWSR Zircaloys. It is thought that the initial hardening of the prismatic planes during cold working is large and thus, the effect of radiation-induced defects remains negligible.

In service, zirconium alloys undergo stress-free radiation growth mainly due to their inherent crystalline anisotropy as well as radiation-enhanced creep under applied stress in addition to thermal creep and elastic deformation. For an example, the post-irradiation examination in Oconee reactor revealed that the stress free axial growth (ε_{zsf}) of cladding followed the relation

$$\varepsilon_{zsf} = 4.9\times10^{-25}\ \phi\ t \tag{13}$$

where the ϕ is fast neutron flux (in neutrons /cm^2-s) and t the time of radiation exposure. Very slight changes were noted in the diametral dimension under unstressed condition (only growth). Therefore, radiation induced creep strain is given by,

$$\varepsilon_{irr} = B\ \phi^{y}\ \sigma\ t \tag{14}$$

where B and y (~1) are material constants. Overall, the total creep strain is given by the addition of the thermal and radiation components.

Application to In-Reactor Performance

Here, we summarize the application to predictions of in-reactor dimensional changes of cladding tubes of CWSR Zircaloy-4 with creep anisotropy using the formulations discussed so far. As noted earlier, creep anisotropy for CWSR Zircaloy is not affected by radiation exposure, and hence, the CODF-Creep model predictions along with modifications through grain shape anisotropy factor can be applied to rationalize the creep data. It can be noted here that radiation growth is highly anisotropic in nature with slight change in diameter. With the various constants determined and optimized from post-irradiation examinations (PIE) along with application of CODF-creep model, it becomes possible to predict dimensional changes in-reactor, as demonstrated by Wilson and co-workers [21]. Here, we summarize the axial length and creep-down results. An excellent correlation has been noted in the changes in axial length following two cycles of irradiation as illustrated in Figure 10a. The predictions of the creep-down as a function of the axial location of 12 Zircaloy-4 fuel rods in the Oconee reactor follow similar trends as observed in PIE (Figure 10b). These correlations show very little effects of axial ratcheting from power cycling and two-point fuel-to-cladding contact on the overall fuel rod length changes. This behavior corresponds well with the axial distribution of clad temperature and flux. The over-prediction of the creep down occurring at the top of the rods is attributed to the presence of two-point contact between the cladding and the fuel-stack, retarding further creep-down. With appropriate finite element analyses, it is also possible to predict the evolution of ovality of the fuel rods [21]. It should be pointed out that the radiation exposure leads to the strengthening of the materials, thus retarding thermal creep. These modifications are necessary when the contribution of thermal creep is comparatively large.

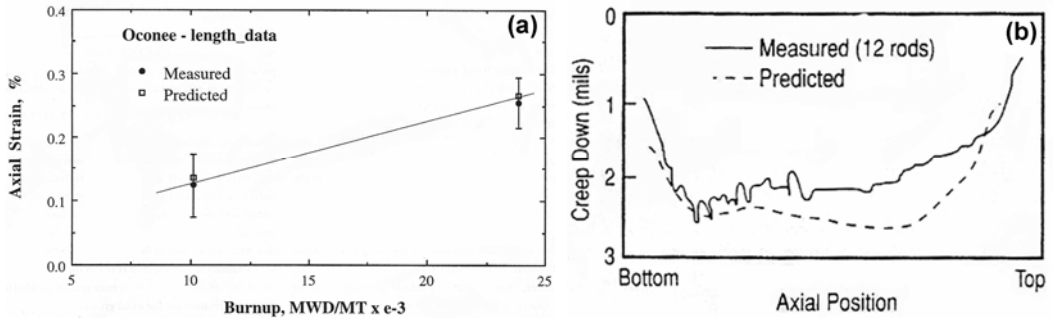

Figure 10. (a) In-pile axial strains versus burn-up (Oconee reactor). (b) In-pile creep down versus axial location fuel rods (Oconee reactor) compared with model predictions

Underground dry storage of spent fuel rods is the preferred method of dealing with waste in the open nuclear fuel cycle currently used in the U.S. During dry storage, the decay heat is removed by gaseous cooling media and thus the temperature remains higher than in wet storage. Hence, the creep deformation and rupture is regarded as the prime degradation mechanism under such conditions. Life estimation based on deformation mechanisms has been made on Zircaloys, and details of the procedure have been described by Zhou et al. [5].

Conclusions

In this study, textural characteristics of Zircaloy-4 and Zirlo have been investigated in terms of direct pole figures and CODF. Biaxial creep testing of these tubings revealed that both materials are inherently anisotropic. Creep loci based on texture data and CODF-Creep model were predicted accurately for recrystallized materials with respect to the experimental one; however, the creep loci prediction for CWSR materials deviated because of the additional stress enhancement occurring during grain boundary sliding. Life prediction methodologies and results are discussed under in-pile and dry storage condition. More studies are called in this regard.

Acknowledgment

This work is supported by the US National Science Foundation through the grants DMR0101309 and DMR0412583. Authors also wish to acknowledge the partial financial support by the DOE-NEER program through grant # DE-FG07-041D14611 for this work.

References

1. H.G. Rickover, "History of Development of Zirconium Alloys for use in Nuclear Power Reactors" (Report US ERDA, NR&D, 1975).
2. K.L. Murty, "Biaxial Creep Behavior of Textured Zircaloy Tubing," *JOM*, February (1992), 49-55.
3. K.L. Murty, "Texture Related Physical, Mechanical and Corrosion Characteristics of Zirconium Alloys: Application to Nuclear Technology," *Textures in Materials Research*, ed. R.K. Ray and A.K. Singh (Hyderabad, India, 1997) 113-157.
4. K.L. Murty, J. Ravi, and Witratmo, "Transitions in Creep Mechanisms and Creep Anisotropy in Zr-1Nb-1Sn-0.2Fe Sheet," *Nuc. Eng. Design*, 156 (1995) 359.
5. Y. Zhou, B. Devarajan, and K.L. Murty, "Short-term Rupture Studies of Zircaloy-4 and Nb-modified Zircaloy-4 tubing using closed-end internal pressurization," *Nuclear Engineering and Design*, 228 (2004), 3-13.
6. J. Yan, "Crystallographic Texture and Creep Anisotropy in Cold Worked and Recrystallized Zirlo" (Ph.D. thesis, North Carolina State University, 2005).
7. H.J. Bunge, "Technological Applications of Texture Analysis," *Zieschrift Metallkunde*, 76 (1985), 457-470.
8. K.L. Murty, "Zircaloy Life Prediction and New Generation Zircaloys for LWRs," *Trans. Indian Inst. Met.*, 50 (1997), 533-562.
9. K.L. Murty and B.L. Adams, "Biaxial Creep of Textured Zircaloy: Part I – Phenomenological and Experimental Descriptions," *Mater. Sci. Eng.*, 70 (1985) 169-180.
10. R. Hill, "A Theory of Yielding and Plastic Flow of Anisotropic Metals", *Proc. Roy. Soc.*, 193A (1948), 281-297.
11. W.A. Backofen, *Deformation Processing,* Addison-Wesley, 1972.
12. K.L. Murty, "Creep Studies for Zircaloy Life Prediction in Water Reactors," *JOM*, October (1999) 32-39.
13. H. Stehle, E. Steinberg and E. Tenckhoff, "Mechanical Anisotropy and Microstructure of Zircaloy Canning Tubes," Zirconium in the Nuclear Industry: Third International Conference, STP 633 (Philadelphia, PA: ASTM, 1977) 486-507.
14. S.T. Mahmood, W.L. Daugherty, and K.L. Murty, "Anisotropic Biaxial Creep of Zircaloy Cladding: Effects of Recrystallization and Neutron Irradiation," Paper no. C0942/C presented at the 10th International Conference of *Structural Mechanics in Reactor Technology* (San Francisco, CA, 1989).
15. D.S. Sarma, K.M. Al-Otaibi and K.L. Murty, "Mechanical Properties and Deformation Structures of a Zirconium-Niobium-Bismuth Alloy," *Metals Materials Processes*, 4 (1992), 217-228.
16. J.C. Earthman et al., "Effects of Grain-Shape Anisotropy and Texture on Balanced-Biaxial Creep of Ti and Zr Alloys," *JOM*, 46 (1994) 48-54.
17. K.L. Murty, B.V. Tanikella, and J.C. Earthman, "Effect of Grain Shape and Texture on Equi-Biaxial Creep of Stress Relieved and Recrystallized Zircaloy-4," *Acta Metall. Mater.*, 42 (1994) 3653-3661.
18. A.J. Ardell and O.D. Sherby, "Steady State Creep of Polycrystalline Alpha Zirconium at Elevated Temperatures," *Trans. AIME*, 239 (1967), 1547-1556.
19. M. Nakatsuka and M. Nagai, *J. Nuc. Sci. Tech.*, 24 (1987) 832.
20. G.S. Clevinger, B.L. Adams, and K.L. Murty, "Analysis of Irradiation Growth and Multiaxial Deformation Behavior of Nuclear Fuel Cladding," *Zirconium in the Nuclear Industry* (4th International Conference), STP 681 (1979) 189.
21. H.W. Wilson et al., "Development and Correlation of Cladding Creep and Irradiation Growth Model", Proceedings of IAEA Specialists Meeting on *Water Reactor Fuel Element Performance Computer Modeling* (Blackpool, UK, 1980).

The grant for this project accomplished what we proposed on Zircaloy cladding by considering the standard Zry-4 and Zirlo. However, we could not procure M5 alloy for similar studies. We also attempted to procure other advanced Zircaloys with no success. We thus took up a detailed review of the creep of Zr-based alloys that was published as a technical paper in the Journal of Nuclear Materials (I. Charit and K.l. Murty, "Creep Behavior of Niobium-Modified Zirconium Alloys," Journal of Nuclear Materials, 374 (2008) 354-363). It would be of significance to extend these types of studies to other cladding materials that have been developed for high burn up conditions in LWRs such as M5 developed and being used by Areva and HANAs developed by KAERI.

The DOE-NEER grant supported a number of graduate students at NC State University mainly in the Nuclear Engineering department. Some of the work was carried out by graduate students in the Materials Science & Engineering department at NCSU working under the supervision of the PI who is a joint appointee between the two departments. Dr. Yan who was partially supported by this grant completed his doctoral degree in Nuclear Engineering and joined Lawrence Berkeley Laboratory as a post doctoral fellow supported by the Virginia Polytechnic Institute. Mr. Brian Marple who was supported by this grant completed his MS degree in Nuclear Engineering and is now employed at Areva Corp. Dr. Srikant Gollapudi who participated in some of the activities completed his doctoral degree in Materials Science & Engineering in 2007 and joined the Defense Metallurgical Laboratory in India. Dr. Indrajit Charit who participated in assisting the graduate students as a post doctoral fellow supported by another grant joined Materials Science and Engineering department at the University of Idaho jointly working at their Nuclear Engineering program at the satellite campus in Idaho Falls.

Relevant Publications and Presentations acknowledging DOE-NEER support:

1. I. Charit, J. Yan, B. Marple and K. Linga Murty, "Effects of Alloying and Thermal Treatment on Creep Anisotropy of Zircaloys: Application to In-Reactor Creep," published in Proceedings of 'Creep Deformation and Fracture, Design, and Life Extension,' edited by R.S. Mishra, J.C. Earthman, S.V. Raj and R. Viswanathan, MS&T'05, Pittsburgh, PA. pp. 41-52. Proceedings of a Symposium Sponsored by Materials Science & Technology 2005 (MS&T'05).
2. G. Srikant, B. Marple, I. Charit and K.L. Murty, "Characterization of stress rupture behavior of cp-Ti via burst testing," Mat Sci Eng. in print.
3. B. Marple, I. Charit, J. Yan, S. Gollapudi, K.L. Murty, "Short-Term Rupture and Biaxial Creep Studies of Recrystallized Zircaloy-4 Tubing," presented at the ANS Winter Meeting, Washington DC, Nov. 2005, 11/14 – 11/17/05.
4. I. Charit and K.L. Murty, "On the Creep Behavior of Nb-modified Zr Alloys," Proceedings of ICAPP '06, Paper 6030, ANS Meeting, Reno, NV, 6/2006.
5. I. Charit and K.L. Murty, "Texture and Creep Anisotropy in Zirconium Alloys," THERMEC06, Vancouver,Canada, July 4-8, 2006 (invited).
6. I. Charit and K.L. Murty, "Structural Materials for Gen-IV Nuclear Reactors: Challenges and Opportunities," in proceedings of International Conference on Advances in Nuclear Materials (ANM06), Mumbai, India, Dec. 12-15 (2006) accepted for publication in J. Nuclear Materials.
7. C.S. Seok, B. Marple, I. Charit and K.L. Murty, "High Temperature Deformation Characteristics of Zirlo^{TM} Tubing via Ring Creep and Burst Tests," presented at the SMiRT 19, Toronto, Canada, Aug 12-17, 2007, paper C02/1.
8. I. Charit and K.L. Murty, "Creep behavior of Nb-containing Zr-Alloys: An Overview," presented at the SMiRT 19, Toronto, Canada, Aug 12-17, 2007, paper C01/1.